FOREX Publication
Open Access | Rapid and quality publishing

International Journal of
Electrical and Electronics Research (IJEER)
Research Article | Volume 14, Issue 2 | Pages 492-506 | e-ISSN: 2347-470X

A New Optimally Designed FOPID Controller for the 3-Area Deregulated Environment Using MWHOA Approach

Saraswathi Sriramula[1*], and B. Ravindranath Reddy[2]

[1]Department of EEE, Research Scholar, JNTU Hyderabad, Telangana, India; Email: saraswathi.maargam@gmail.com
[2]Department of EEE, Deputy Executive Engineer, JNTU Hyderabad, Telangana, India; Email: bumanapalli_brreddy@yahoo.co.in

***Correspondence:** *Saraswathi Sriramula; saraswathi.maargam@gmail.com*

ABSTRACT- This work proposes a metaheuristic optimization approach for AGC in deregulated power systems. The analysis is carried out on a 3-AMS comprising gas turbine power plants, hydroelectric, thermal power stations and wind energy units. The primary objective is to reduce ACE, which includes tie-line power deviations and frequency fluctuations, under different operating conditions. To achieve optimal performance, a MWHOA is employed to determine the optimal gain parameters of FOPID. The proposed strategy evaluates the dynamic performance of generators in a 3-AMS under a deregulated environment. It emphasizes the significance of optimizing the FOPID controller to ensure system stability, with the ITAE used as the performance index. Furthermore, the effectiveness of the proposed method is validated by comparing its performance with that of PSO. The effectiveness of the proposed method is further evaluated through various case studies, including Poolco and bilateral transaction scenarios, along with stability and sensitivity analyses. The comparative analysis demonstrates that the MWHOA-optimized FOPID controller delivers superior performance over other methods, particularly in regulating generator outputs, minimizing tie-line power variations, and maintaining frequency stability across multi areas. The obtained ITAE value for the transient response is 0.0005497, and the settling time in case-1 Poolco agreement using the MWHOA optimized controller is 10.10 seconds. Nevertheless, these numbers are lower than what PSO was able to attain. Comparing case-2, the bilateral settling time is 10.23 seconds, and ITAE is 0.0004491 less than PSO and other methods found in the literature.

Keywords: Fractional-order proportional–integral–derivative controller, Modified whale optimization, integral of time-weighted absolute error, deregulated power system, frequency fluctuations and tie-line power deviations.

ARTICLE INFORMATION

Author(s): Saraswathi Sriramula, and B. Ravindranath Reddy;
Received: 17/03/26; **Accepted**: 24/05/26; **Published**: 30/06/26;
E- ISSN: 2347-470X;
Paper Id: IJEER 1703B16;
Citation: 10.37391/ijeer.140225
Webpage-link:
https://ijeer.forexjournal.co.in/archive/volume-14/ijeer-140225.html

Publisher's Note: FOREX Publication stays neutral with regard to jurisdictional claims in Published maps and institutional affiliations.

1. INTRODUCTION

Since it is difficult to get a remote system, the only option available in the modern period is an interconnected electrical power network. An interconnected power system consists of multiple utilities operating together as a unified network. Variations in load demand can cause the system to deviate from its normal operating conditions, and these deviations must be controlled within acceptable limits to ensure reliable operation. To maintain system stability, the generated power must continuously match the demand. Any imbalance between generation and load leads to frequency deviations and fluctuations in tie-line power.

1.1. Motivation and Research Gap

Traditional PI/PID controllers and many recently developed optimization -based approaches exhibit several shortcomings, including low resilience, inadequate adaptability to stochastic renewable energy source variations, slow convergence characteristics, susceptibility to premature trapping in local optima, and weak performance under both bilateral and Poolco market environments. These issues emphasize the necessity for a robust optimization mechanism coupled with a highly adaptive control strategy. To mitigate these limitations, this study introduces an MWHOA-optimised FOPID controller. Bio-inspired PID controllers are capable of providing superior adaptability and effective nonlinear dynamic handling; however, they often face challenges related to mathematical rigour and practical implementation. Conversely, FOPID controllers ensure strong theoretical stability and better industrial feasibility, but their adaptability remains limited under uncertain and dynamic operating conditions. Therefore, the identified gap motivates the development of hybrid control frameworks that combine the adaptive intelligence of bio-inspired optimization methods with the robustness and reliability of FOPID control architecture.

2. LITERATURE SURVEY

LFR plays a vital role in maintaining system stability by ensuring that tie-line power deviations and frequency variations remain within specified limits. In a deregulated setting, the coordination of generating, transmission, and distribution companies is supervised by an independent system operator. With increasing load demand and continuous expansion of power networks, maintaining system frequency has become a critical concern in modern power systems.

FOREX Publication
Open Access | Rapid and quality publishing
International Journal of Electrical and Electronics Research (IJEER)
Research Article | Volume 14, Issue 2 | Pages 492-506 | e-ISSN: 2347-470X

Conventional power systems typically comprise nuclear, hydro, and thermal generating units. When there is a mismatch between power generation and load demand, the system deviates from its nominal operating condition. To address this issue, LFC is essential for maintaining system stability. Consequently, numerous researchers have investigated LFC strategies across different power system configurations.

The authors in [4] highlighted the roles of key entities such as GENCOs, TRANSCOs, and DISCOs. Several single-area power system models were presented in [5]. The impact of generator excitation on system performance has been examined, and the damping methods that provide frequency stability under various load circumstances are covered in [6]. Furthermore, [7] focuses on AGC, where ACE is utilized to regulate power flow through continuous monitoring of frequency, tie-line power and generator output.

The study in [8] examines the impact of an ideal output feedback controller in a hybrid power system. Additionally, [9] incorporates energy storage components to enhance load frequency control performance and introduces a novel cost function to address LFC challenges. In practice, single-area systems are insufficient, making LFR in multi-area systems inevitable. The stability of such multi-area power systems largely depends on effective control design and optimization techniques. A comprehensive review of multi-area power systems from both LFR and AGC perspectives is presented in [10].

Arya et al. [11] discussed the design challenges associated with a fuzzy-based AGC scheme for a two-area power system. In [12], a gradient-based tuned PI controller was applied to a four-area power system, demonstrating improved performance over other control methods in maintaining voltage, Δf, and ΔPtie under various operating conditions. A decentralized control approach based on sliding mode control has also been proposed. Furthermore, to minimise the ITAE criterion, [13] introduced a novel Coati Optimization Algorithm to enhance the performance of a TID+IDN controller in a 3-area hybrid system operating under deregulated conditions.

To further improve system dynamics and stability, Aribowo et al. [14] proposed a modified Mountain Gazelle Optimization algorithm for tuning PID controller gains in DC motor applications. In a subsequent study [15], the same authors emphasized the importance of precise parameter tuning by employing a gradient-based optimization technique for PID control of DC motors. Collectively, these works underline the critical role of optimization techniques in enhancing controller performance across diverse engineering applications.

The authors of [16] examined the optimal operation and control strategies for hybrid power systems. Furthermore, [17] introduced a novel RIME algorithm for security-constrained load dispatch, taking into account the uncertainties inherent in power systems.

In [18], a unique model order reduction technique combined with fuzzy logic control was presented to simplify controller design, effectively lowering system complexity while keeping important dynamic properties. In another study, [19] used a sinh-cosh optimization approach for aircraft pitch control, resulting in increased stability and faster responsiveness. Furthermore, [20] proposed an optimally tuned Fractional Order PID controller utilizing the Aquila Optimizer to improve system performance by reducing ACE. Besides, different optimization methods were adopted for AI, FOPID controller to maintain stability and power quality of the power system [21-29]. Lastly, the whale optimization was used for cyber-attack in system and energy management [30].

2.1. Research Contributions

However, *table 1* clearly indicates that most of the previously published studies primarily concentrated on two-area power systems incorporating conventional and renewable energy sources with traditional LFC strategies.

This work focuses on load frequency regulation in a three-area multi-source system using an optimized FOPID controller. The main contribution lies in applying the Modified Whale Optimization Algorithm (MWHOA) to achieve optimal tuning of controller parameters in a hybrid power system. This innovative method's output is evaluated under various system operating settings, demonstrating how well it enhances controller performance. The challenge of enhancing PS performance containing a variety of energy sources, including thermal, hydro, gas, and wind, is specifically taken into consideration in the work that is proposed. The performance of the proposed controller is evaluated through a comparative study with a PSO-tuned FOPID controller. This work's significant contributions are as follows:

- Development of an MWHOA-based optimized FOPID controller to address load frequency control challenges in a deregulated interconnected three-area multi-source system.
- Application of the MWHOA-tuned FOPID controller to a hybrid 3-AMS comprising both renewable and conventional generation units for effective LFC management.
- Modelling and simulation of the three-area multi-source system with diverse generating units using the MATLAB/Simulink platform.
- Evaluation of system performance under both bilateral and Poolco market structures.
- Comparative analysis with a conventional optimization technique, such as PSO, to demonstrate the effectiveness of the proposed approach.

The remainder of the paper is organized as follows: *Section 3* describes the structure of the 3-AMS. *Section 4* presents the design of the MWHOA-optimized FOPID controller for addressing the load frequency control problem in a deregulated environment. *Section 5* discusses the simulation results obtained from multiple case studies in detail and also examines the stability and convergence behavior of the proposed controller. Finally, *Section 6* concludes the paper.

FOREX Publication
Open Access | Rapid and quality publishing
International Journal of Electrical and Electronics Research (IJEER)
Research Article | Volume 14, Issue 2 | Pages 492-506 | e-ISSN: 2347-470X

Table 1. State of Art of Literature

S. No.	Reference Number	Traditional LFC/ Deregulated LFC	Controller	Type of Area	Renewable Energy (RE) /Conventional (C)	Metaheuristic Algorithm considered
1	13	Deregulated	TID + IDN	3	RE+C	Coatis optimization
2	15	Traditional	2DOF-PID-FOI	2	RE+C	Improved Squirrel
3	20	Deregulated	FOPID	2	RE+C	Aquila Optimization
4	27	Traditional	FOPI(1+PDN)	2	RE+C	Spider Wasp Optimizer
5	Proposed	Deregulated	FOPID	3	RE+C	Modified whale optimization

3. CONSTRUCTION OF DEREGULATED 3-AMS

The mathematical representation of the 3-AMS considered for AGC in a deregulated environment is illustrated in *figure 1*. This system serves as the foundation for analysing AGC performance under restructured conditions. The model comprises different types of generating units distributed across three areas. In Area1, thermal, wind, and hydro power plants are included. Area2 consists of thermal, hydro, and gas-based generating units, while Area3 incorporates thermal, hydro, and wind energy systems. To maintain *Δf* and *ΔPtie* within acceptable limits, a FOPID controller is implemented in each area.

Each control area contains three DISCOs, resulting in a total of 9 number of GENCOs and 9 number of DISCOs in the restructured system. Power transfers among GENCOs and DISCOs inside the same control area are referred to as Poolco-based exchanges, whereas bilateral transactions occur between entities belonging to different areas. The contractual power participation between GENCOs and DISCOs is defined using the DPM. In this matrix, the number of columns represents the DISCOs, and the number of rows corresponds to the GENCOs. Every column in the DPM has a sum of elements that always equals unity. GENCOs 1-3 & DISCOs 1-3 are located in Area1; GENCOs 4-6 & DISCOs 4-6 are located in Area2; and GENCOs 7-9 & DISCOs 7-9 are located in Area3. *Equation (1)* presents the corresponding DPM (13).

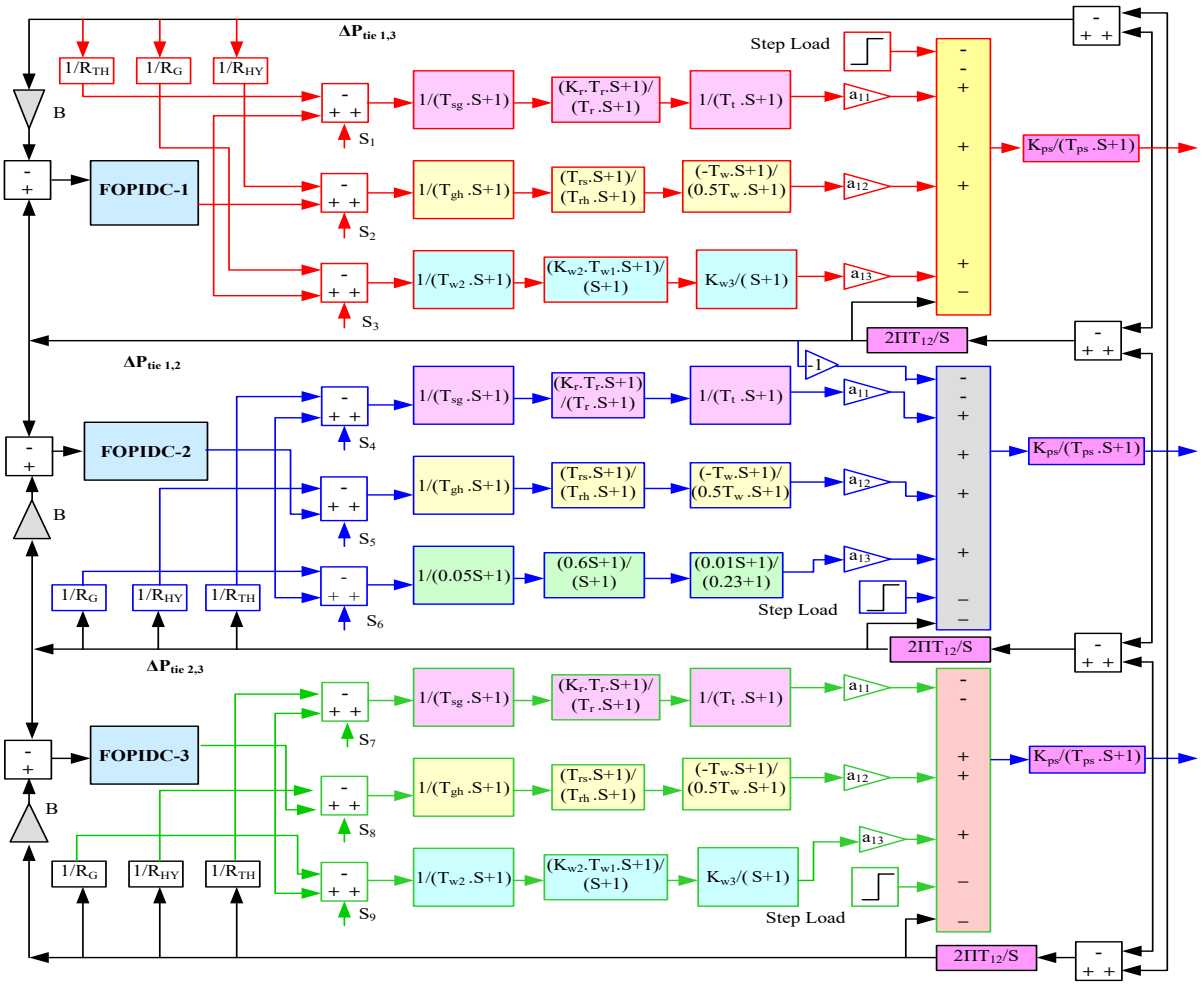

Figure 1. 3-AMS transfer function

FOREX Publication
Open Access | Rapid and quality publishing
International Journal of Electrical and Electronics Research (IJEER)
Research Article | Volume 14, Issue 2 | Pages 492-506 | e-ISSN: 2347-470X

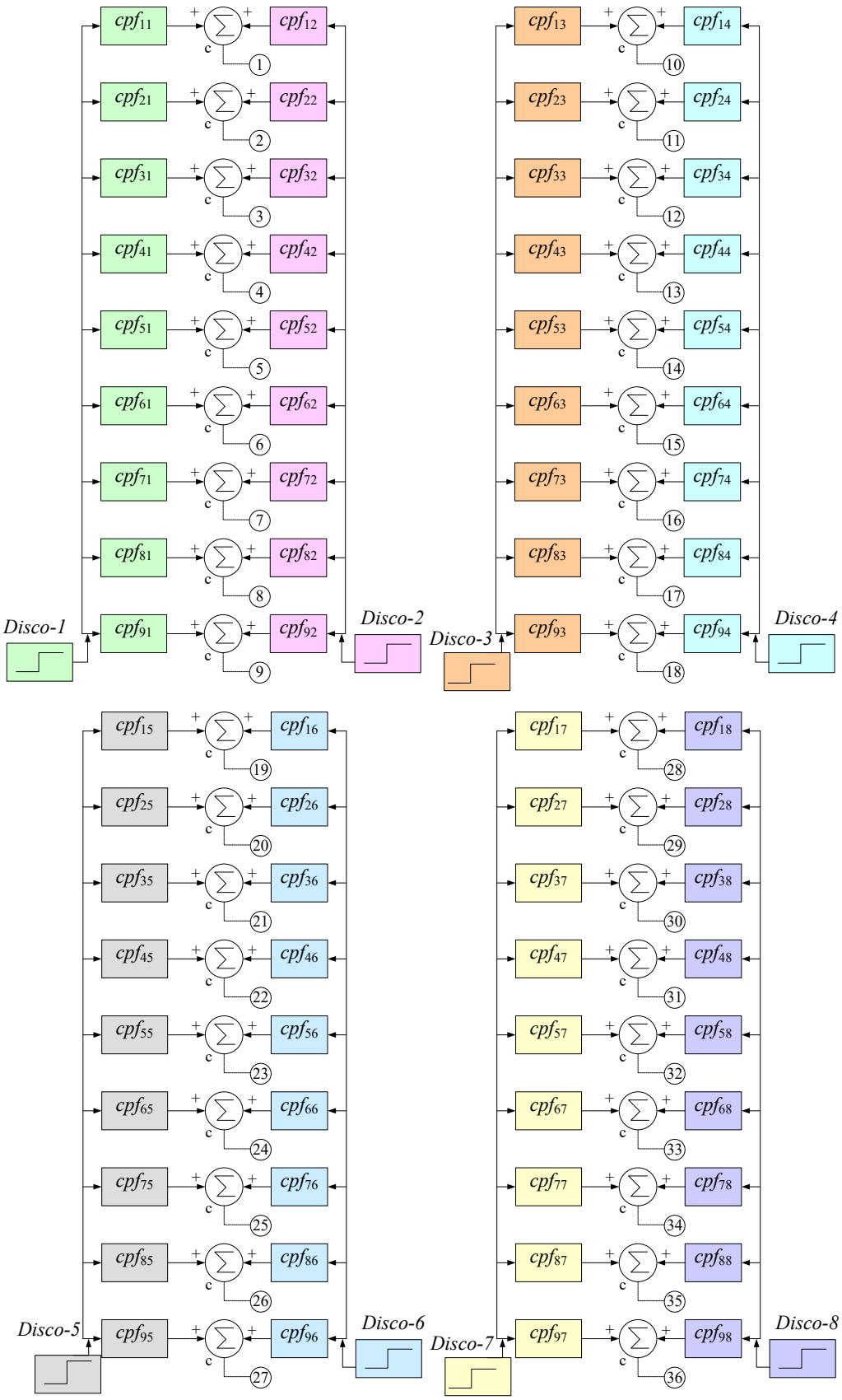

Figure 2. DISCOs and GENCOs' CPF

FOREX Publication
Open Access | Rapid and quality publishing
International Journal of Electrical and Electronics Research (IJEER)
Research Article | Volume 14, Issue 2 | Pages 492-506 | e-ISSN: 2347-470X

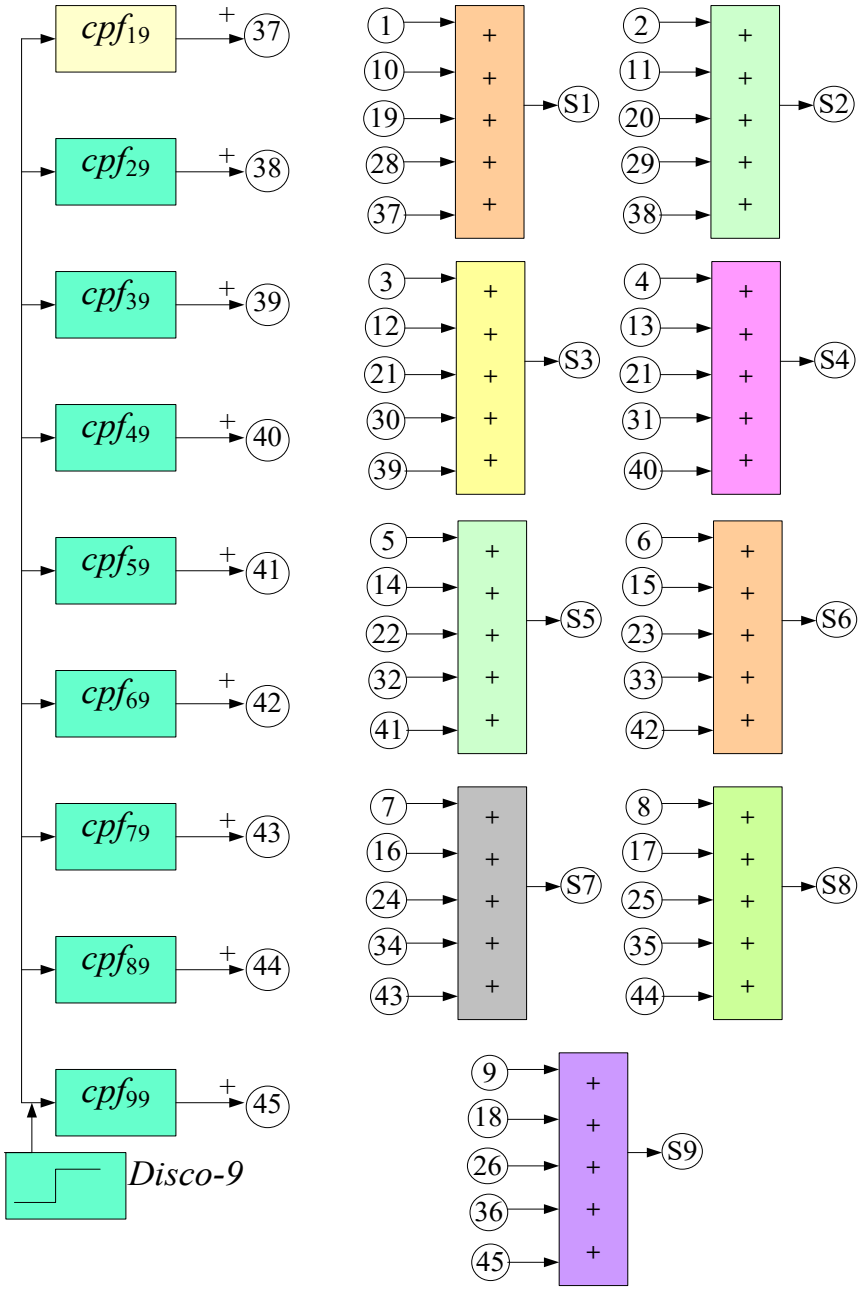

Fig 2: Cont….

$$DPM = \begin{bmatrix} cpf_{11} & cpf_{12} & cpf_{13} & cpf_{14} & cpf_{15} & cpf_{16} & cpf_{17} & cpf_{18} & cpf_{19} \\ cpf_{21} & cpf_{22} & cpf_{23} & cpf_{24} & cpf_{25} & cpf_{26} & cpf_{27} & cpf_{28} & cpf_{29} \\ cpf_{31} & cpf_{32} & cpf_{33} & cpf_{34} & cpf_{35} & cpf_{36} & cpf_{37} & cpf_{38} & cpf_{39} \\ cpf_{41} & cpf_{42} & cpf_{43} & cpf_{44} & cpf_{45} & cpf_{46} & cpf_{47} & cpf_{48} & cpf_{49} \\ cpf_{51} & cpf_{52} & cpf_{53} & cpf_{54} & cpf_{55} & cpf_{56} & cpf_{57} & cpf_{58} & cpf_{59} \\ cpf_{61} & cpf_{62} & cpf_{63} & cpf_{64} & cpf_{65} & cpf_{66} & cpf_{67} & cpf_{68} & cpf_{69} \\ cpf_{71} & cpf_{72} & cpf_{73} & cpf_{74} & cpf_{75} & cpf_{76} & cpf_{77} & cpf_{78} & cpf_{79} \\ cpf_{81} & cpf_{82} & cpf_{83} & cpf_{84} & cpf_{85} & cpf_{86} & cpf_{87} & cpf_{88} & cpf_{89} \\ cpf_{91} & cpf_{92} & cpf_{93} & cpf_{94} & cpf_{95} & cpf_{96} & cpf_{97} & cpf_{98} & cpf_{99} \end{bmatrix} \quad (1)$$

FOREX Publication
Open Access | Rapid and quality publishing
International Journal of Electrical and Electronics Research (IJEER)
Research Article | Volume 14, Issue 2 | Pages 492-506 | e-ISSN: 2347-470X

The *cpf* specifies the contribution level of each generator to the overall system response. The tie-line power deviations among the areas are denoted by ΔP_{12}, ΔP_{23}, and ΔP_{31}, while the frequency deviations in Areas1, 2, and 3 are represented by ΔF_1, ΔF_2, and ΔF_3, respectively.

$$cpf_{ij} = \frac{jthDISCOpowerdemandfromjthGENCO}{jthDISCO'stotalpowerdemand} \quad (2)$$

The Areas 1, 2, and 3 tie-line power exchanges can be determined using *equations (3)– (5)*, which are formulated based on the cpf.

$$\Delta P_{12} = \sum_{i=1}^{3}\sum_{j=4}^{6} cpf_{ij}\Delta P_{Lj} - \sum_{i=4}^{6}\sum_{j=1}^{3} cpf_{ij}\Delta P_{Lj} \quad (3)$$

$$\Delta P_{23} = \sum_{i=4}^{6}\sum_{j=7}^{9} cpf_{ij}\Delta P_{Lj} - \sum_{i=7}^{9}\sum_{j=4}^{6} cpf_{ij}\Delta P_{Lj} \quad (4)$$

$$\Delta P_{31} = \sum_{i=7}^{9}\sum_{j=1}^{3} cpf_{ij}\Delta P_{Lj} - \sum_{i=1}^{3}\sum_{j=7}^{9} cpf_{ij}\Delta P_{Lj} \quad (5)$$

Eq. (6-8) gives the actual power transfer across the tie line between control regions 1, 2, and 3.

$$\Delta P_{12} = \frac{2\Pi T_{12}}{s}(\Delta F_1(s) - \Delta F_2(s)) \quad (6)$$

$$\Delta P_{23} = \frac{2\Pi T_{23}}{s}(\Delta F_2(s) - \Delta F_3(s)) \quad (7)$$

$$\Delta P_{31} = \frac{2\Pi T_{31}}{s}(\Delta F_3(s) - \Delta F_1(s)) \quad (8)$$

Under steady-state conditions, the deviation in tie-line real power is expected to be zero. Any mismatch is treated as an error, as expressed in *equation (9)*, to evaluate the ACE, Accordingly, ACE can be defined as:

$$ACE_i = Bi\Delta F_{ierror} + \Delta P_{ierror} \quad (9)$$

Equation (10) describes the objective function:

$$ITAE = \int_0^t (|\Delta F_1| + |\Delta F_2| + |\Delta F_3| + |\Delta P_{tie(1-2)}| + |\Delta P_{tie(2-3)}| + |\Delta P_{tie(3-1)}|).t.dt \quad (10)$$

4. PROPOSED MWHOA TUNED FOPIDC

In this work, an MWHOA FOPID controller is employed to address LFC Problem in a 3-AMS. The Modified Whale Optimization Algorithm is utilized to achieve optimal tuning of controller parameters in the hybrid test system. The next subsections provide a detailed description of the proposed MWHOA technique and the FOPID controller design.

4.1. Modified Whale Optimization Algorithm

Proposals have been made to modify the algorithm with the aim of improving the current WHOA's speed and convergence rate. It has been shown that self-enhancement can be useful in traditional optimization methods. This is a quick description of the mathematical representation of the proposed MWHOA.

Prey Encircling: The whales have the ability to find their target and make loops over it. In a search space, D refers to the dimension and N is the whale population size, the location of the i^{th} whale is denoted as $R_i = (R_{i,1}, R_{i,2}, \ldots, R_{i,G})$; $i \in 1, 2, \ldots, N$. The present best position is considered as the prey in the population. While other members of the population travel toward the best individual for encirclement, whale individuals approach the target prey to encircle. The humpback whales' surrounding movements [30] are given by *equations (11)* and *eq. (12)*, where the continuous iteration is indicated by and the coefficient vectors.

$$\vec{G} = |\vec{H}.\vec{R}_p(t) - \vec{R}(t)| \quad (11)$$

$$\vec{R}(t+1) = \vec{R}_p(t) - \vec{B}.\vec{G} \quad (12)$$

Here, the current iteration is denoted by t. R(t) is the position vector of the current individual; $\vec{R}$ stands for the prey's position. Moreover,$\vec{R}$, $\vec{R}_p$indicates both the location vector and the greatest position thus far discovered. Furthermore, $\vec{B}$and$\vec{H}$are calculated with the help of *equations (13)* and *(14)*. For varying iterations, the component in *equation (15)* drops from 2 to 0. The interval [0, 1] contains the randomly generated vectors and positions.

$$\vec{B} = 2a.r_1 - \vec{a} \quad (13)$$

$$\overrightarrow{H} = 2ra_2 \quad (14)$$

Here, an is the convergence factor, which progressively drops from 2 to 0 with an increasing number of iterations; r1 and r2 are random values in the interval [0, 1].

(i) Exploitation Phase: The modeling in this phase is based on the "Shrinking encircling mechanism and Spiral updating position."

(a) Encircling shrinking system: This was achieved by reducing the value in *equation (15)*.
(b) New Spiral updates Evaluation with Tri-level: *Equation (14)* creates a spiral formula based on the prey's and i^{th} whale's positions. $\vec{G}$indicates the distance between the two, l is an integer that lies between and b is a parameter that determines the logarithmic spiral shape. The mathematical expression for is provided by *equation (16)*.

$$R(t+1) = \vec{G}'\, e^{bl}.Cos(2\pi l) + \vec{R}_p(t) \quad (15)$$

$$\vec{G'} = |\vec{R}_p(t) - \vec{R}(t)| \quad (16)$$

FOREX Publication
Open Access | Rapid and quality publishing
International Journal of Electrical and Electronics Research (IJEER)
Research Article | Volume 14, Issue 2 | Pages 492-506 | e-ISSN: 2347-470X

Equation (17), which displays whale locations numerically throughout optimization,

$$R(t+1) = \begin{cases} \vec{R}_p(t) - \vec{B}.\vec{G} & if \quad \varphi < 0.5 \\ \vec{G''}.e^{bl}.Cos(2\pi l) + \vec{R}_p(t) & if \quad \varphi \geq 0.5 \end{cases} \quad (17)$$

This version incorporates the regular update evaluation together with a novel tri-level update. The values φ_1, φ_2, φ_3 are initialized. If, $\varphi < 0.5$ then the values and are determined by applying *eqs. (14) and (12)*. On the other hand, φ_3 is calculated by *equation (15)*. *Equation (16)* is then used to update the search agent position after a random variable's $ran \leq 0.3$ value has been initialized. If the search agent's present position $ran = 0.3\ to\ 0.6$ is changed in line with *equation (17)*. *Equation (18–20)* modifies the current search agent position in the event that these two prerequisites are not met. The selected method is referred to as MWHOA since there are three stages of updating.

$$\vec{R}(t+1) = \frac{\varphi_1 + \varphi_2}{2} \quad (18)$$

$$\vec{R}(t+1) = \frac{\varphi_2 + \varphi_3}{2}, \quad (19)$$

$$\vec{R}(t+1) = \vec{X}_{(rand)} - \vec{B}.\vec{G}, \quad (20)$$

(ii) Search for Prey (Exploration Phase): *Equations (21)* and *(22)* provide an evaluation for the search for prey (exploration phase). The vector denoting the random location selected from the existing population is symbolized by $X_{(rand)}$

$$\vec{G} = \left|\vec{H}\,\vec{R}_{(rand)} - \vec{R}\right|, \quad (21)$$

$$\vec{R}(t+1) = \vec{X}_{(rand)} - \vec{B}.\vec{G} \quad (22)$$

(iii) Pseudocode of MWHOA:

START with the agents that are randomly generated R_i (i=1, 2, 3...., N)
Evaluate the fitness of each search agent (SA)
R= best SA*
WHILE (t <t_{max})
FOR every SA
    Revise a, B, H, l, and φ
IF (φ<0.5)
    IF(|B|<1)
    Revise the position of SA use Eq. (11)
    ELSE IF (|B|>1)
    Pick a random SA (R)
    Revise the position of SA use Eq. (17)
    END IF
ELSE IF (φ>0.5)
    Revise the position by Eq. (15) spiral
END IF
END FOR
    Check if any SA goes beyond the search space and amend it
Evaluate the fitness of the obtained solutions
Update R if not the global best solution*
t=t+1
END WHILE
*RETURN R**

4.2. FOPID Controller

Various AGC controllers have been developed and implemented in previous studies. In recent years, fractional-order controllers have gained significant attention due to their enhanced noise suppression capability and reduced computational complexity compared to conventional controllers. The structure of the FOPID controller [21], illustrated in *figure 3*, is defined by five parameters: *Kp*, *Ki*, K_d, μ, and λ. The controller output is described by a differential equation, and its corresponding transfer function $G_c(t)$ is given in *equation (23)*.

$$Gc(t) = \frac{Y(s)}{U(s)} = K_p + K_i\frac{1}{S^{\lambda}} + K_d S^{\mu} \quad (23)$$

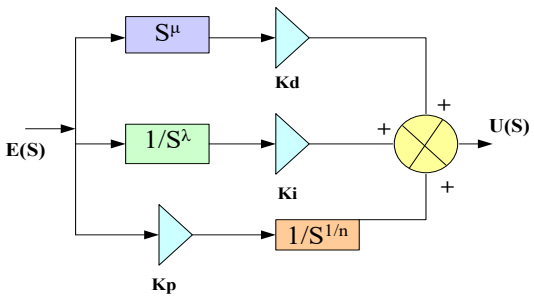

Figure 3. FOPID controller

The gain parameters of the FOPID controller are treated as the decision variables in the optimization problem. Accordingly, in the EWHOA framework, each whale is represented as a vector that encodes these variables as follows:

$$R = \left[K_p, K_i, K_d, \lambda, \mu\right], \quad (24)$$

The limitations are shown as

$$R_{i_{\min}} \leq R_i \leq R_{i_{\max}}; i = 1,2.3..n, \quad (25)$$

The *fitness (F)* can be constructed using the constraints and the normalized objective functions, which give each selected objective equal weight and consider both minimization and maximization functions.

$$\text{Max F} = \frac{1}{1+(\text{Obj})}, \quad (26)$$

$$Obj = ITAE \quad (27)$$

The design variables are subject to specific bounds and constraints, which must be satisfied during the optimization process. Therefore, these limitations are incorporated while determining the optimal solution. Accordingly, the objective of the present optimization problem is to minimize the ITAE criterion, subject to the following constraints:

FOREX Publication
Open Access | Rapid and quality publishing
International Journal of Electrical and Electronics Research (IJEER)
Research Article | Volume 14, Issue 2 | Pages 492-506 | e-ISSN: 2347-470X

$$\begin{aligned} K^{Min}{}_p \le K_P \le K^{Max}{}_p, \\ K^{Min}{}_d \le K_d \le K^{Max}{}_d, \\ K^{Min}{}_i \le K_i \le K^{Max}{}_{i,} \\ \lambda^{Min} \le \lambda \le \lambda^{Max}, \\ \mu^{Min} \le \mu \le \mu^{Max}, \end{aligned} \quad (28)$$

In *equation (28)*, the terms Min and Max denote the lower and upper bounds of the controller parameters. To ensure effective optimization, appropriate ranges are assigned to the design variables. In this study$(K_p, K_i, K_d)$are constrained within 0 to 2, while the fractional integral and derivative orders$(\mu, \lambda)$are limited to the range of 0 to 1.

The fractional-order operators (s^{λ}) and (s^{μ}) of the FOPIDC are implemented using the Oustaloup Recursive Approximation technique. A fifth-order approximation is selected to achieve an effective trade-off between computational efficiency and approximation accuracy. The approximation is carried out over a frequency range of 10^{-3} to 10^{3} rad/s, which sufficiently captures the dominant dynamics of the AGC system. All simulations are performed with a sampling time of 0.01 s.

The optimization process is continued until the convergence criteria are satisfied, resulting in an MWHOA-tuned FOPIDC capable of providing fast dynamic response, reduced Area Control Error (ACE), and improved system robustness. Compared with several conventional optimization algorithms, MWHOA offers a well-balanced exploration and exploitation capability; however, it may impose a relatively higher computational burden when dealing with multi-objective optimization problems. In this work, the MWHOA is implemented with a population size of 25 search agents and a maximum of 100 iterations. Each optimization run requires an average computation time of about 25–30 seconds on a standard desktop system with an Intel i7 processor and 16 GB of RAM.

5. RESULTS AND DISCUSSIONS

The 3-AMS considered in this study is modeled in MATLAB, as illustrated in *figure 1*, for load frequency control analysis. The optimal parameters of the FOPID controller are determined by the proposed MWHOA method. For comparison, a PSO-tuned FOPID controller is also implemented to evaluate the dynamic response. Different power transaction scenarios between GENCOs and DISCOs are analyzed within the framework of a deregulated market. Both Poolco and bilateral agreements are considered while examining multiple case studies. The effectiveness of the LFC strategy is evaluated through these scenarios, as discussed in the subsequent sections.

Case I: POOLCO Agreement

In this scenario, all GENCOs within the three areas participate equally in AGC. A load disturbance of 0.033 per unit (p.u.) is applied in area 1 and distributed equally among the three DISCOs within that control area. Additionally, the DISCOs in other control areas do not provide any load to the GENCOs.

$$DPM = \begin{bmatrix} 0.333 & 0.333 & 0.333 & 0 & 0 & 0 & 0 & 0 & 0 \\ 0.333 & 0.333 & 0.333 & 0 & 0 & 0 & 0 & 0 & 0 \\ 0.333 & 0.333 & 0.333 & 0 & 0 & 0 & 0 & 0 & 0 \\ 0 & 0 & 0 & 0 & 0 & 0 & 0 & 0 & 0 \\ 0 & 0 & 0 & 0 & 0 & 0 & 0 & 0 & 0 \\ 0 & 0 & 0 & 0 & 0 & 0 & 0 & 0 & 0 \\ 0 & 0 & 0 & 0 & 0 & 0 & 0 & 0 & 0 \\ 0 & 0 & 0 & 0 & 0 & 0 & 0 & 0 & 0 \\ 0 & 0 & 0 & 0 & 0 & 0 & 0 & 0 & 0 \end{bmatrix} \quad (29)$$

In particular, the existence of null values in the appropriate cells in the DPM given by *eq. (29*) shows that there are no contractual agreements between a GENCO and a DISCO of two different control regions. The following is an evaluation of the power generated by several GENCOs.

ΔP_{g1}=0.0099, ΔP_{g2}=0.0099, ΔP_{g3}=0.0099, ΔP_{g4}=ΔP_{g5}= ΔP_{g6}= ΔP_{g7}= ΔP_{g8}= ΔP_{g9}= 0.

Under steady-state conditions, the power generated by each GENCO should match the demand of the DISCOs within its respective area. *Figures 4* and *5* illustrate the tie-line power flows among the three areas as well as the frequency deviations in each region. Furthermore, *table 2* presents key time-domain performance metrics—such as settling time, undershoot, and overshoot—for both the proposed method and the PSO-based approach in the Poolco case study. In addition, *table 3* provides the optimized FOPID controller parameters obtained using different optimization techniques, along with their corresponding objective values.

Table 2. Time-domain performance characteristics for Case1

Method	Parameters	Undershoot	Overshoot	Settling time
PSO	ΔF_1	-0.0450	0.010	18.71
	ΔF_2	-0.00520	0.00065	21.62
	ΔF_3	-0.00530	0.0012	22.13
	ΔP_{12}	-0.00190	0.009	18.02
	ΔP_{23}	-0.00180	0.0082	20.13
	ΔP_{31}	-0.00020	0.021	18.37
MWHOA	ΔF_1	-0.0310	0.010	10.10
	ΔF_2	-0.0040	0.00041	13.42
	ΔF_3	-0.00430	0.00090	12.43
	ΔP_{12}	-0.00221	0.0087	16.72
	ΔP_{23}	-0.00223	0.0082	18.91
	ΔP_{31}	-0.00010	0.0197	15.12

Figures 4 and *5* demonstrate the improved performance of the MWHOA-optimized FOPID controller. The proposed approach exhibits a faster and smoother response to variations in tie-line power and frequency compared to other controllers. It effectively suppresses oscillations in both Δf and ΔP_{tie} during transient conditions. The generator output responses for *Case I* are in *figures 6* and *7*. The results clearly indicate that the MWHOA-tuned FOPID controller outperforms the PSO-based approach. Additionally, *Figure 8* shows the convergence behavior of both methods, highlighting the superior efficiency and faster convergence of the proposed optimization technique.

FOREX Publication
Open Access | Rapid and quality publishing
International Journal of
Electrical and Electronics Research (IJEER)
Research Article | Volume 14, Issue 2 | Pages 492-506 | e-ISSN: 2347-470X

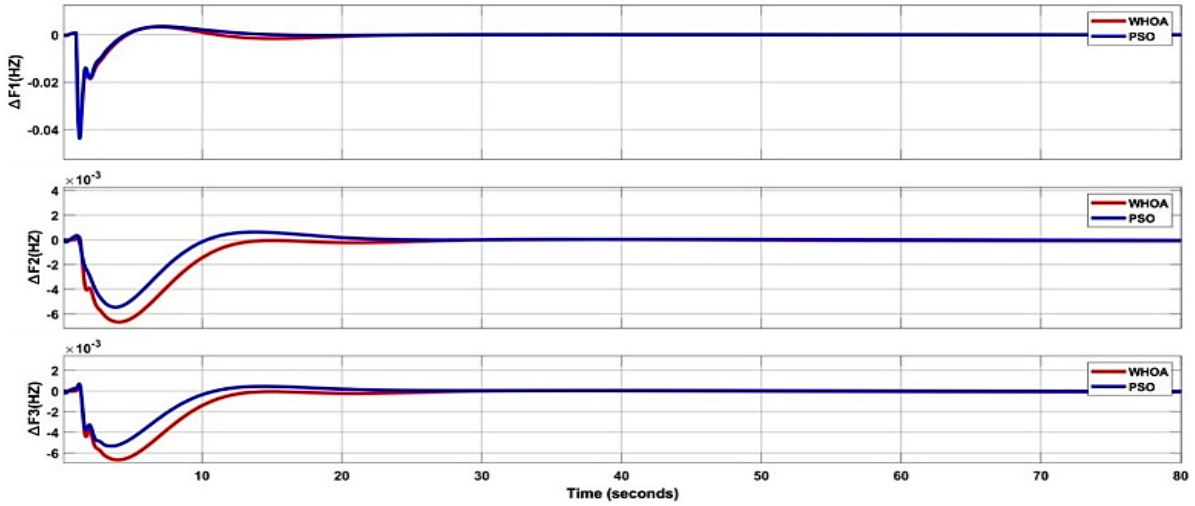

Figure 4. Comparison of frequency deviations for Case 1

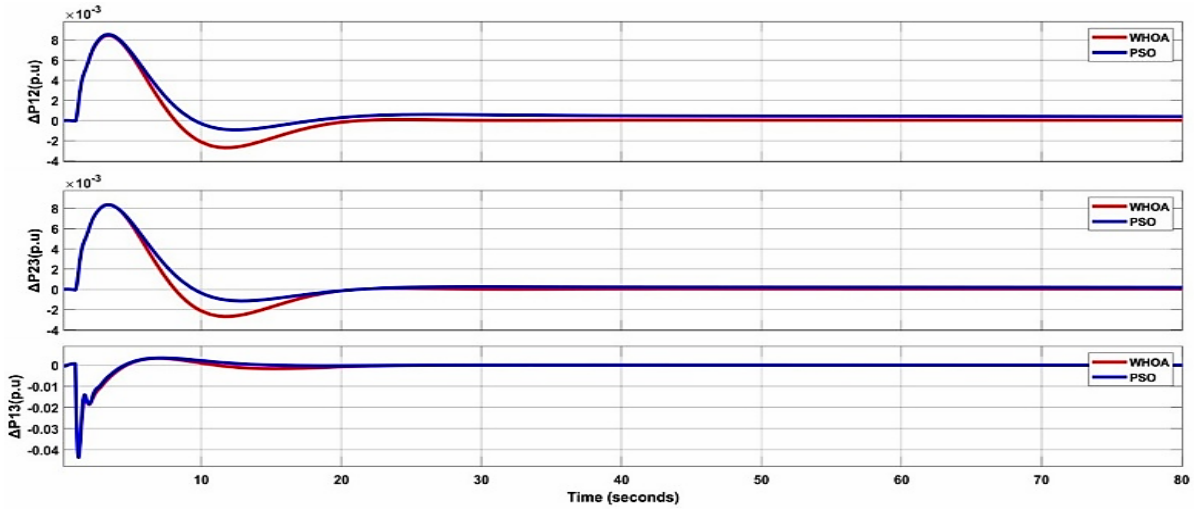

Figure 5. Comparison of tie-line power responses for Case 1

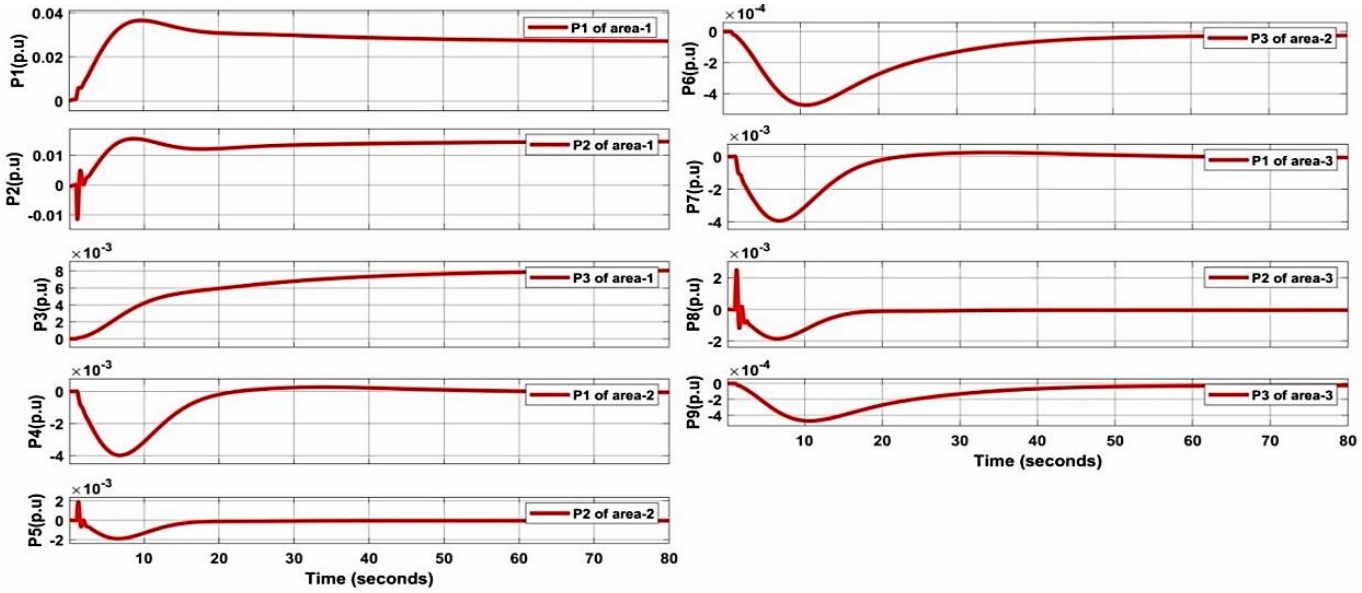

Figure 6. Power generation response of the MWHOA-based approach for Case 1

FOREX Publication
Open Access | Rapid and quality publishing
International Journal of Electrical and Electronics Research (IJEER)
Research Article | Volume 14, Issue 2 | Pages 492-506 | e-ISSN: 2347-470X

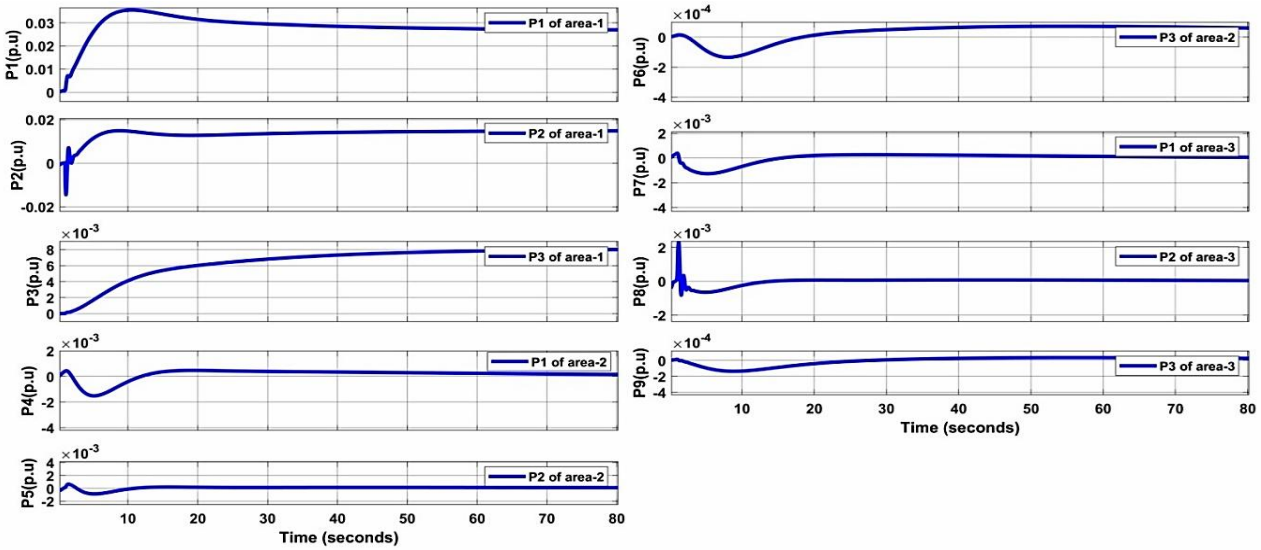

Figure 7. Power generation response using the PSO-based approach for Case 1

Table 3. Optimally tuned controller gains for Case 1

Method	Objective (ITAE)	Gain parameters	Controller -1	controller-2	controller-3
PSO	0.0005579	K_p	1.369	1.4514	1.1924
		K_i	1.5	0.11127	0.2195
		K_d	0.857	0.1	1.3206
		λ	0.7869	0.7869	0.7869
		μ	0.85	0.6789	0.923
MWHOA	0.0005497	K_p	1.1001	1.441	1.5
		K_i	1.5	0.6730	0.6831
		K_d	0.7067	1.1923	1.5
		λ	0.855	0.8559	0.8559
		μ	0.7446	0.9345	0.7289

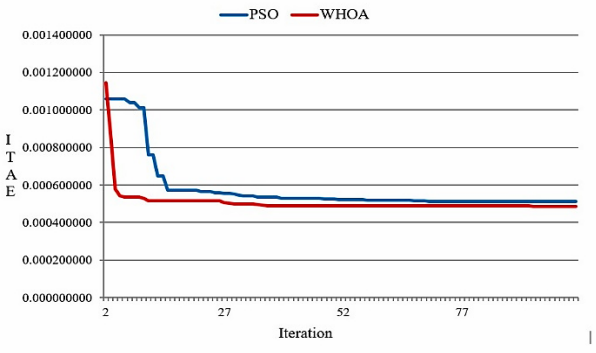

Figure 8. Convergence characteristics for Case 1

Case study II: Bilateral agreement

In this scenario, DISCOs in any area can procure power from GENCOs located in any other region. Based on the transactions assigned by the system operator, each GENCO adjusts its generation to meet the demand of the participating DISCOs. The corresponding DISCO Participation Matrix (DPM) for bilateral transactions is given as follows:

$$DPM = \begin{bmatrix} 0.1 & 0.1 & 0.2 & 0.1 & 0.1 & 0.1 & 0.2 & 0.2 & 0.3 \\ 0.1 & 0.1 & 0.1 & 0.1 & 0.1 & 0.1 & 0.1 & 0.2 & 0 \\ 0.1 & 0.1 & 0.1 & 0.1 & 0.2 & 0.1 & 0.1 & 0.1 & 0.1 \\ 0.2 & 0.1 & 0.1 & 0.2 & 0.1 & 0.2 & 0.1 & 0.1 & 0 \\ 0.1 & 0.1 & 0.1 & 0.1 & 0.1 & 0.1 & 0.1 & 0 & 0.2 \\ 0.1 & 0.1 & 0.1 & 0.1 & 0.1 & 0.1 & 0.1 & 0.05 & 0.2 \\ 0.1 & 0.2 & 0.1 & 0.1 & 0.1 & 0.1 & 0.1 & 0.05 & 0 \\ 0.1 & 0.1 & 0.1 & 0.1 & 0.1 & 0.1 & 0.1 & 0.1 & 0.1 \\ 0.1 & 0.1 & 0.1 & 0.1 & 0 & 0.1 & 0.1 & 0.2 & 0.1 \end{bmatrix} \quad (30)$$

In this scenario, the three-area power system operates under a bilateral transaction framework. Load variations are introduced across all DISCOs in each area, with Area1 experiencing a total load change of 0.03 p.u., and similar variations are applied to the other areas. In Area1, DISCOs 1, 2, and 3 each demand 0.01 p.u. Likewise, in Area2, DISCOs 4, 5, and 6 each require 0.01 p.u. In Area3, DISCOs 7, 8, and 9 also have individual demands of 0.01 p.u.

The DPM is formulated based on the contractual agreements established between GENCOs and DISCOs. Based on these agreements, the generation outputs of the GENCOs are determined. The corresponding changes in generation, ΔPg1 to ΔPg9, are calculated as 0.014, 0.009, 0.01, 0.011, 0.009, 0.0095, 0.0085, 0.009, and 0.01, respectively.

The time-domain response characteristics are summarized in *table 4*, clearly indicating that the proposed controller significantly reduces overshoot and undershoot. *Table 5* presents the optimal controller parameter values obtained using different optimization techniques, evaluated based on the ITAE index.

Table 4. Time-domain performance characteristics for Case 2

Method	Parameters	Undershoot	Overshoot	Settling time
PSO	ΔF_1	-0.045	0.009	12.72
	ΔF_2	-0.0042	0.0018	35.61
	ΔF_3	-0.0052	0.0012	19.92

FOREX Publication
Open Access | Rapid and quality publishing
International Journal of Electrical and Electronics Research (IJEER)
Research Article | Volume 14, Issue 2 | Pages 492-506 | e-ISSN: 2347-470X

	ΔP_{12}	-0.0012	0.0102	35.10
	ΔP_{23}	-0.00135	0.0089	20.64
	ΔP_{31}	-0.0423	0.09	15.55
MWHOA	ΔF_1	-0.052	0.002	10.23
	ΔF_2	-0.0037	0.0023	30.04
	ΔF_3	-0.0048	0.0012	17.84
	ΔP_{12}	-0.0017	0.0072	32.94
	ΔP_{23}	-0.00134	0.0071	19.17
	ΔP_{31}	-0.0440	0.0062	15.12

Figures 9 and *10* present the responses of Δf and ΔP_{tie} respectively. It is evident that, under the bilateral transaction scenario, the proposed MWHOA-tuned FOPID controller outperforms other controllers. This improvement is reflected in reduced settling time and effectively suppressed oscillation magnitudes during both rising and falling responses. Furthermore, *Figure 13* shows that the MWHOA-based FOPID controller achieves superior performance compared to the PSO-based method. The generator power outputs for *Case II* are illustrated in *figures 11* and *12*.

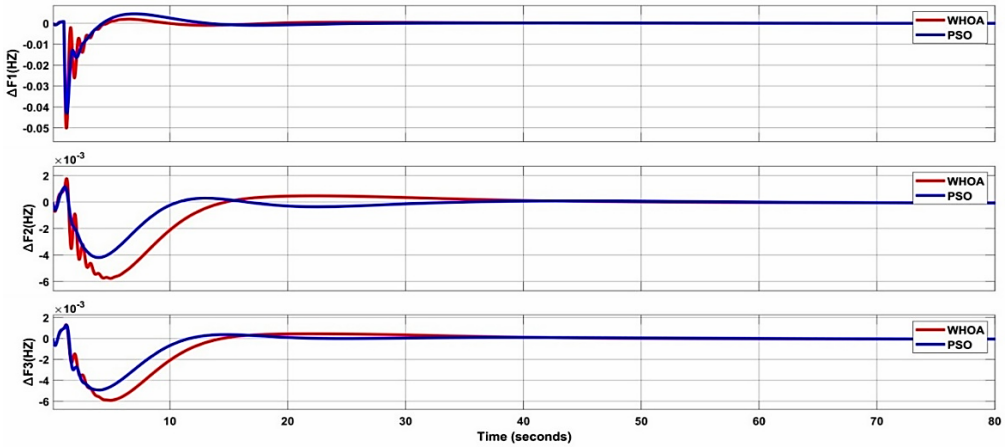

Figure 9. Comparison of frequency deviations for case2

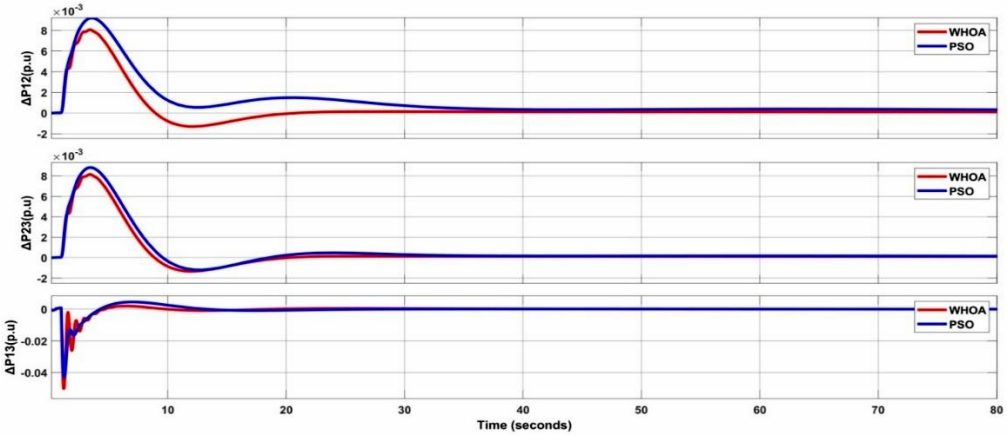

Figure 10. Comparison of tie-line power responses for case2

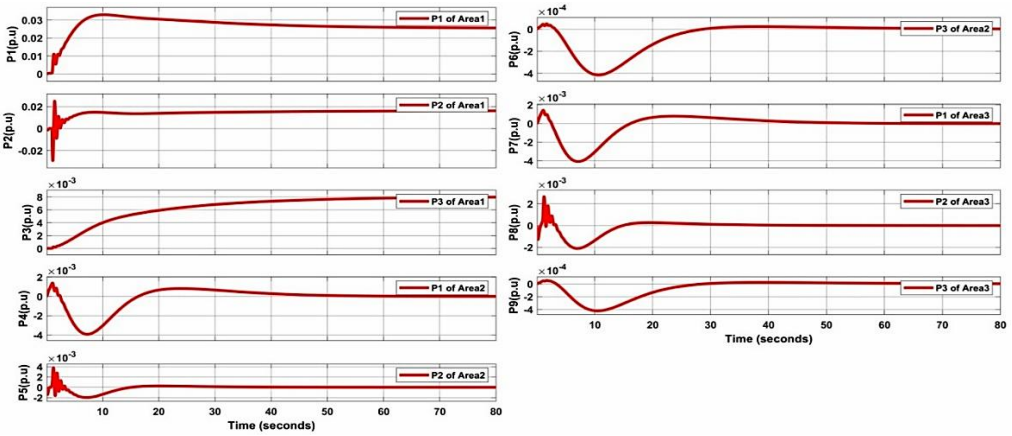

Figure 11. Power generation response of the MWHOA-based approach for case 2

FOREX Publication
Open Access | Rapid and quality publishing
International Journal of Electrical and Electronics Research (IJEER)
Research Article | Volume 14, Issue 2 | Pages 492-506 | e-ISSN: 2347-470X

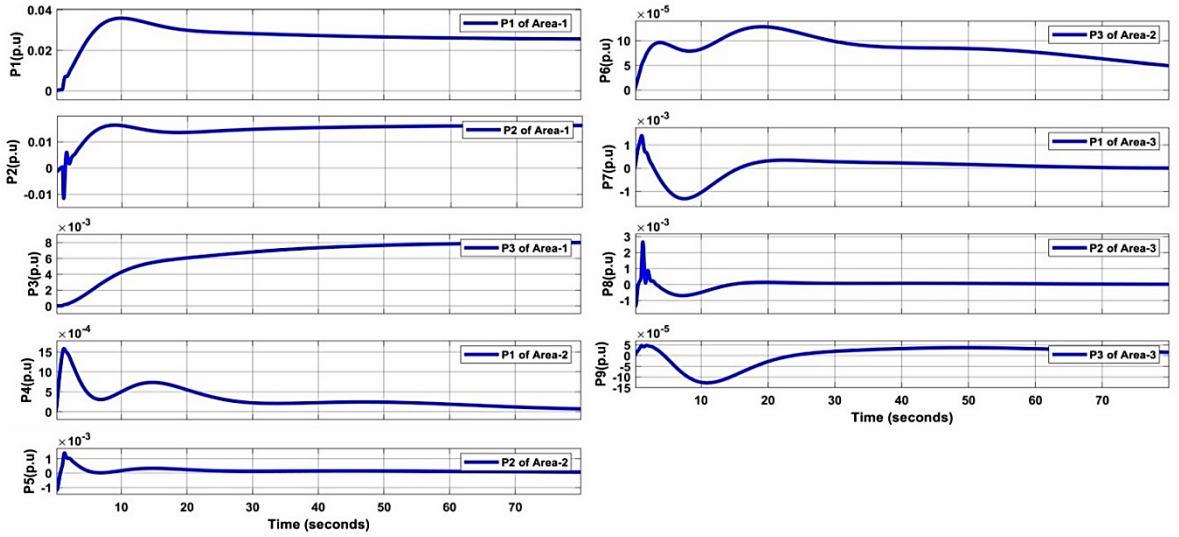

Figure 12. Power generation response using the PSO-based approach for case2

Table 5. Optimally tuned controller gains for Case 2

Method	Objective (ITAE)	Gain Parameters	Controller-1	Controller-2	Controller-3
PSO	0.0004509	K_p	1.489	1.495	1.26
		K_i	1.5	1.498	1.43
		K_d	1.029	1.5	0.648
		λ	0.743	0.741	0.745
		μ	0.80	0.926	0.823
MWHOA	0.0004491	K_p	1.5	0.233	0.348
		K_i	1.5	1.5	1.5
		K_d	1.5	0.104	1.5
		λ	0.756	0.756	0.7563
		μ	0.7140	0.980	0.650

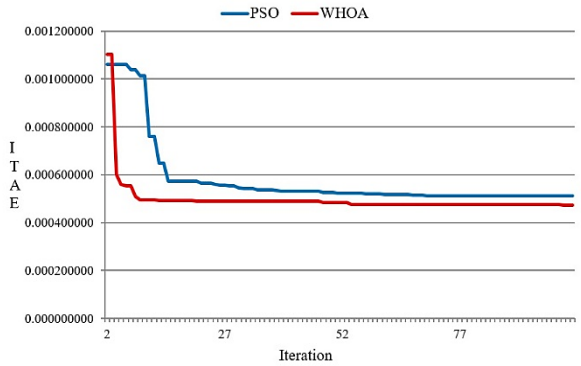

Figure 13. Convergence comparison plot of case2

Table 6 shows the superior performance of the proposed method compared to methods that are available in the literature survey. Furthermore, *table 7* provides the statistical analysis of ITAE carried out for *Case-1* and *Case 2*, with the best, mean and worst values with standard deviation for 20 runs. The suggested method offers better robustness against market-driven power exchanges, renewable intermittency, as well as increased tuning flexibility and speedier convergence.

Table 6. Settling time comparison with techniques published in the literature

Reference [No]	Case	Optimized-Controller	Settling Time (sec)
[13]	1	COA- IDN	13.64
[13]		SSA- TID + IDN	11.69
[13]		COA- TID	12.48
[13]		PSO- TID + IDN	14.17
Proposed		**MWHOA-FOPIDC**	**10.10**
[13]	2	COA- IDN	13.53
[13]		SSA- TID + IDN	12.14
[13]		COA- TID	11.13
[13]		PSO- TID + IDN	24.95
Proposed		**MWHOA-FOPIDC**	**10.23**

Case III: Frequency Domain Stability Test

The stability analysis of the MWHOA-tuned FOPID controller is presented in *figures 14* and *15*. Frequency-domain techniques, such as Bode plots and Nyquist diagrams, are widely used to evaluate the stability characteristics of load frequency control systems. These tools provide important insights into the system behavior by examining magnitude and phase responses, from which gain margin, phase margin, crossover frequencies, phase shifts, and resonance characteristics can be determined. A stable system is characterized by a positive gain margin and a phase margin greater than zero degrees. In this study, the load frequency control design is focused on improving these stability margins to enhance overall system performance. The results obtained from the Bode analysis confirm that both gain and phase margins are positive, indicating that the system remains stable.

FOREX Publication
Open Access | Rapid and quality publishing
International Journal of Electrical and Electronics Research (IJEER)
Research Article | Volume 14, Issue 2 | Pages 492-506 | e-ISSN: 2347-470X

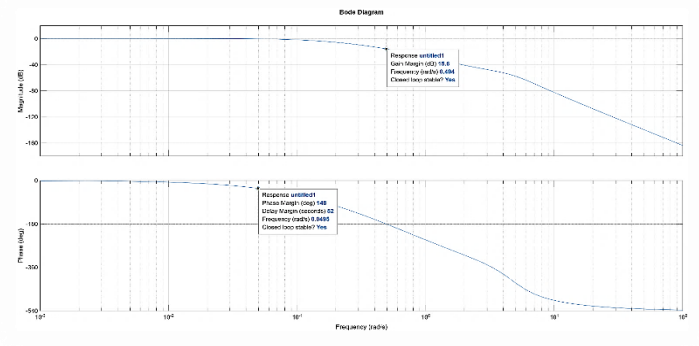

Figure 14. Bode plot of the MWHOA-based controller

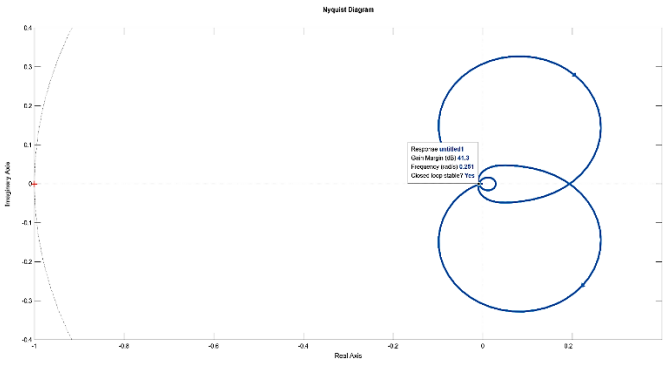

Figure 15. Nyquist plot for MWHOA

Table 7. Statistical Analysis of objective function for case studies for 25runs

Case number	Best ITAE	Mean ITAE	Worst ITAE	Standard Deviation
1	0.0005497	0.0005599	0.0005789	$1.49*10^{-5}$
2	0.0004491	0.0004501	0.0004607	$1.37*10^{-5}$

Case IV: Sensitivity analysis

Since an ideal power system model cannot be achieved under practical operating conditions, the robustness of the MWHOA-tuned FOPID controller against parameter uncertainties and nonlinearities must be thoroughly evaluated. For this purpose, three significant system parameters—the governor time constant, frequency bias factor, and speed droop characteristic are independently varied within ±40% of their nominal values provided in the Appendix. The corresponding system performance indices under different operating scenarios, along with the associated MWHOA-optimized controller parameters, are presented in *table 8*.

Table 8. Sensitivity Analysis Using the Suggested Approach and Variations in Power System Parameters in Area1

Parameter variation	% change	Settling time(sec)		
		ΔF_1	ΔF_2	ΔF_3
Nominal	0	10.10	13.42	12.43
*T*gov	+40%	10.08	12.92	11.13
	-40%	10.12	12.76	12.09
R	+40%	10.099	13.415	12.244
	-40%	10.099	13.46	12.56
β	+40%	9.981	13.456	12.41
	-40%	9.854	13.144	12.21

Further examination of *table 8* reveals that the performance indices exhibit only minor variations despite considerable changes in system parameters. In addition, *Figure 16* illustrates the frequency deviation responses of Area-1 for different values of T_{gov}, R, and β, demonstrating that variations in system dynamics have a negligible effect on the control performance when the proposed controller is employed. Overall, the obtained results validate the robustness of the proposed control approach and confirm its ability to ensure stable and reliable operation under substantial parameter uncertainties and nonlinear operating conditions.

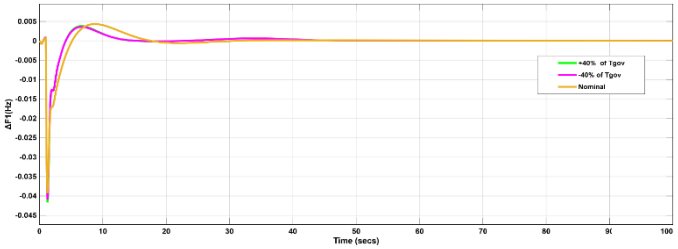

(a) T_{gov}

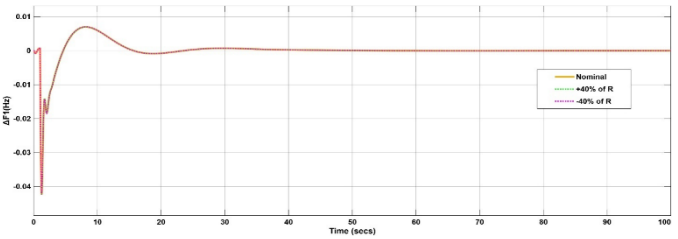

(b) R

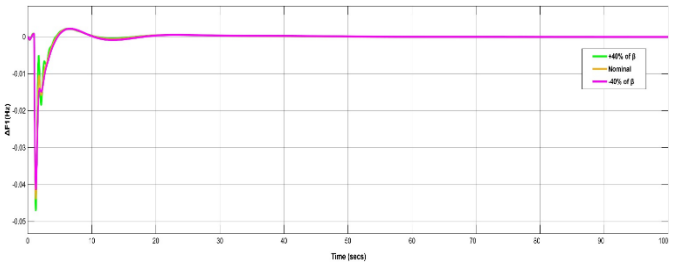

(c) B

Figure 16. Effect of power system parameter variations on the Area-1 frequency response (sensitivity analysis) of Area-1 with the proposed method

Table 9. Tuned parameters of the proposed controller under system parameter variation

Parameter variation	% change	Parameter	Area 1	Area 2	Area 3
*T*gov	+40%	K_p	1.456	1.344	1.691
		K_i	1.561	0.5647	0.7374
		K_d	1.189	0.2643	1.54256
		λ	0.8039	0.8116	0.86334
		μ	0.7935	0.9238	0.7565
	-40%	K_p	1.4612	1.543	1.246
		K_i	1.413	1.264	0.889
		K_d	1.852	0.775	1.545
		λ	0.651	0.865	0.559
		μ	0.779	0.575	0.784

FOREX Publication
Open Access | Rapid and quality publishing
International Journal of Electrical and Electronics Research (IJEER)
Research Article | Volume 14, Issue 2 | Pages 492-506 | e-ISSN: 2347-470X

R	+40%	K_p	1.4591	0.6458	1.3275
		K_i	1.51	0.8879	0.6452
		K_d	0.5273	1.201	0.9542
		λ	0.8043	0.8075	0.8974
		μ	0.947	0.7543	0.8654
	-40%	K_p	1.52	1.53	1.365
		K_i	1.371	0.4919	0.6707
		K_d	1.065	0.3756	0.1475
		λ	0.8446	0.8449	0.8345
		μ	0.7521	0.6528	0.7548
β	+40%	K_p	0.784	1.14	0.9773
		K_i	1.57	1.3402	0.9672
		K_d	1.369	0.988	0.7658
		λ	0.7767	0.7467	0.7767
		μ	0.9082	0.9702	0.8717
	-40%	K_p	1.189	1.954	0.8018
		K_i	1.149	0.8977	0.7516
		K_d	1.012	0.6343	0.8369
		λ	0.8176	0.8456	0.4567
		μ	0.7943	0.7953	0.9237

6. CONCLUSION

To regulate frequency deviations in a three-area power system, this study proposes a Modified Whale Optimization Algorithm (MWHOA) for optimal tuning of FOPID controller gain parameters. The results demonstrate that the proposed method outperforms the PSO-based approach in a deregulated environment. Simulation outcomes confirm its superior performance for load frequency control in the three-area system. In terms of time-domain performance, the MWHOA-tuned FOPID controller achieves improved settling times for ΔF1, ΔF2, ΔF3 and ΔP12, ΔP23, ΔP31. For the Poolco case, the settling times are 10.10 s, 13.42 s, 12.43 s, 16.72 s, 18.91 s, 15.12 s, respectively. For the bilateral case, the corresponding values are 10.23 s, 30.04 s, 17.84 s, 32.94 s, 19.17 s, 15.12 s, respectively. The proposed controller also significantly reduces peak overshoot and undershoots during transient disturbances. Overall, the results confirm the effectiveness of the proposed approach in improving system performance. The robustness of the control strategy is further validated through frequency-domain stability analysis using Bode plots. However, this work does not consider FACTS devices for stability, multiple area load variation, which can be considered as future work with additional sources recently trending like hydrogen energy and other storage with electric vehicles in the hybrid system.

Nomenclature

Symbol	Description
FOPID	Fractional Order Proportional- Integral- Derivative Controller.
MWHOA	Modified Whale Optimization Algorithm
GENCO	Generation Companies
TRANSCO	Transmission Companies
DISCO	Distribution Companies
DPM	Disco Participation Matrix
RES	Renewable Energy Source
PSO	Particle Swarm Optimization
LFR	Load Frequency Regulation
LFC	Load Frequency Control
3-AMS	Three-Area Multi-Source System
AGC	Automatic Generation Control
cpf	Contract Participation Factor
Δf_i	Frequency Deviation Of Area I (Hz)
ΔP_m	Change In Mechanical Power (Pu)
ΔP_e	Change In Electrical Power (Pu)
ΔP_L	Load Disturbance (Pu)
ΔP_{tie}	Tie-Line Power Deviation (Pu)
ACE	Area Control Error Of Area
B	Frequency Bias Constant
R	Speed Regulation Parameter
K	Power System Gain
T_p	Power System Time Constant (Sec)
T_{gov}	Governor Time Constant (Sec)
T_t	Turbine Time Constant (Sec)
ΔP_g	Governor Output Change (Pu)
K_p	Proportional Gain
K_i	Integral Gain
K_d	Derivative Gain
λ	Fractional Integral Order
μ	Fractional Derivative Order
u(t)	Control Input Signal
e(t)	Error Signal (ACE)
ΔP_{RES}	Total Renewable Power Variation
ΔP_{wind}	Wind Power Variation
ΔP_{solar}	Solar PV Power Variation
T_{RES}	Renewable Energy Time Constant
K_{RES}	Renewable Energy Gain
J	Objective Function
ITAE	Integral Of Time-Weighted Absolute Error
ISE	Integral Square Error
N	Number Of Search Agents
MaxIter	Maximum Iterations
X	Solution Vector
X*	Best Optimal Solution
A	Exploration Coefficient In Optimization Algorithm
C	Position Update Coefficient
a	Linearly Decreasing Parameter Controlling Convergence

Appendix A

The system parameters considered in this study are as follows: $P_R = 2000$MW, $P_L = 1000$MW,$T_{G1} = 0.2$s$f = 60$Hz, , $T_{G2} = 0.3$s, $T_{T1} = 0.5$s, $T_{T2} = 0.5$s, $K_1 = 0.30$, $T_R = 10$s, $T_{RH} = 28.70$s, $T_{CH} = 0.2$s, $T_W = 1$s, $K_{pc} = 0.8$, $K_T = 0.5747$, $K_D = 16.5$, $K_D = 0.2873$, $K_W = 0.138$, $T_{Wd1} = 0.041$s, $T_{Wd2} = 0.6$s, $K_{Wd1} = 1.25$, $K_{Wd2} = 1.3$, $D_1 = 0.6$, $D_2 = 0.9$, $H_1 = 5$, $H_2 = 5$, $K_{DG} = 16.5$, $T_D = 0.025$s, $a_{12} = -1$, $K_p = 1/D$, $T_p = 2H/(Df')$, $R_{T1} = R_{H1} = R_{G1} = 0.05$Hz/p.u., $R_{T2} = R_{H2} = R_{G2} = 0.0625$Hz/p.u., $K_2 = 0.85$, $K_3 = 0.095$, $K_4 = 0.92$, $C_{BD} = 200$, $K_{BD} = 0.03$, $T_{BD} = 26$s, $T_{RBD} = 69$s, $T_{DM} = 0$, and $T_{FD} = 10$s

The simulation is carried out with a sampling time of 0.01s and a total simulation time of 120s, using a variable-step solver (ode45).

Author Contributions: Saraswathi Sriramula: paper drafting writing original draft, investigation, methodology, software, analysis. B. Ravindranath Reddy; Review and editing, supervision and validation.

Conflicts of Interest: "The authors declare no conflict of interest."

FOREX Publication
Open Access | Rapid and quality publishing
International Journal of Electrical and Electronics Research (IJEER)
Research Article | Volume 14, Issue 2 | Pages 492-506 | e-ISSN: 2347-470X

REFERENCES

[1] Majid Zare-Bahramabadi, Hossein Farzin, Mehdi Ehsan, A mixed integer linear programming model for risk-based remote-controlled switches, distributed generation, and tie line placement in distribution systems with complex topologies to improve the resilience, IET Renew. Power Gener. 17 (2023) 2149–2159. https ://doi.org/10.1049/rpg2.12718.

[2] Babu Ram, Sanjeev Kumar Bhagat Naladi, Lalit Chandra Saikia, Tirumalasetty Chiranjeevi, Ramesh Devarapalli, Fausto Pedro García M´arquez, A comprehensive review of recent strategies on automatic generation control/load frequency control in power systems, Arch. Comput. Methods Eng. 30 (1) (2023) 543–572.

[3] R.D. Christie, A. Bose, Load frequency control issues in power system operation after deregulation, IEEE Trans. Power Syst. 11 (1996) 1191–2000.

[4] H.M. Manjunatha, T.S. Karibasavaraju, L.H. Anjaneya, Chandraiah Shadaksharaiah, P. Arunkumar, Auction based single buyer energy trading model in grid-tied microgrid with active sellers and buyers, in: E-Prime- Advances in Electrical Engineering, Electronics and Energy, 2023 100136.

[5] V. Moorthi, R. Aggarwal, Damping effects of excitation control in load-frequency control system, Proc. Inst. Electr. Eng. 121 (1974) 1409–1416.

[6] G. Kusic, J. Sutterfifield, A. Caprez, J. Haneline, B. Bergman, Automatic generation control for hydro systems, IEEE Trans. Energy Convers. 3 (1988) 33–39.

[7] Irfan Ahmed Khan, Hazlie Mokhlis, NurulafiqahNadzirah Mansor, Hazlee Azil Illias, LilikJamilatulAwalin, Li Wang, New trends and future directions in load frequency control and flexible power system: a comprehensive review, Alex. Eng. J. 71 (2023) 263–308.

[8] K.S. Parmar, S. Majhi, D.P. Kothari, Load frequency control of a realistic power system with multi-source power generation, Int. J. Electr. Power Energy Syst. 42 (1) (2012 Nov 1) 426–433.

[9] Emre Çelik, Nihat ¨Oztürk, Essam H. Houssein, Improved load frequency control of interconnected power systems using energy storage devices and a new cost function, Neural Comput. Appl. 35 (1) (2023) 681–697.

[10] Xinghua Liu, Siwei Qiao, Zhiwei Liu, A survey on load frequency control of multi-area power systems: recent challenges and Strategies, Energies 16 (5) (2023) 2323.

[11] Yogendra Arya, Narendra Kumar, AGC of a two-area multi-source power system interconnected via AC/DC parallel links under restructured power environment, Optim. Control Appl. Methods 37 (4) (2016) 590–607.

[12] T. Ali, S.A. Malik, A. Daraz, M. Adeel, S. Aslam, H. Herodotou, Load frequency control and automatic voltage regulation in four-area interconnected power systems using a gradient-based optimizer, Energies 16 (2023) 2086, https://doi. org/10.3390/en16052086.

[13] Dei, G., Gupta, D.K., Sahu, B.K. et al. A novel TID + IDN controller tuned with coatis optimization algorithm under deregulated hybrid power system. Sci Rep 15, 4838 (2025). https://doi.org/10.1038/s41598-025-89237-0

[14] Aribowo, W., Abualigah, L., Oliva, D. &Prapanca, A. A novel modified mountain gazelle optimizer for tuning parameter proportional integral derivative of DC motor. Bull. Electr. Eng. Inf. 13 (2), 745–752 (2024).

[15] Widi Aribowo, R. et al. Controlling parameters proportional integral derivative of DC motor using a gradient-based optimizer. Int. J. Power Electron. Drive Syst. (IJPEDS) 15 (2), 696–703 (2024).

[16] Premkumar, M. et al. Optimal operation and control of hybrid power systems with stochastic renewables and FACTS devices: an intelligent multi-objective optimization approach. Alexandria Eng. J. 93, 90–113 (2024).

[17] Pandya, S. B. et al. Multi-objective RIME algorithm-based techno economic analysis for security constraints load dispatch and power flow including uncertainties model of hybrid power systems. Energy Rep. 11, 4423–4451 (2024).

[18] Alsmadi, O., Abu-Hammour, Z. &Mahafzah, K. Digital systems model order reduction with substructure preservation and fuzzy logic control. Eurasia Proc. Sci. Technol. Eng. Math. 28, 14–22 (2024).

[19] Abualigah, L., Ekinci, S. &Izci, D. Aircraft pitch control via filtered proportional-integral-derivative controller design using Sinh Cosh optimizer. Int. J. Rob. Control Syst. 4 (2), 746–757 (2024).

[20] Deepak Kumar Gupta, Geetanjali Dei, Ankit Kumar Soni, Amitkumar V. Jha, Bhargav Appasani, Nicu Bizon, Avireni Srinivasulu, Philibert Nsengiyumva, Fractional order PID controller for load frequency control in a deregulated hybrid power system using Aquila Optimization, Results in Engineering, Volume 23, 2024,102442, https://doi.org/10.1016/j.rineng.2024.102442.

[21] Srilakshmi, K., Kondreddi, K., Ramadevi, A. et al. Grid connected and standalone renewable source fed UPQC: a hybrid control technique for power quality enhancement. Discov Appl Sci 7, 147 (2025). https://doi.org/10.1007/s42452-025-06562-9

[22] Srilakshmi, K., Pandian, A. N., &Palanivelu, A. (2024). Fuzzy Based Hybrid Controller for UPQC with Wind and Battery Storage Systems. International Journal of Electronics, 111(10), 1800 –1825.

[23] Srilakshmi, K., Santosh, D.T., Ramadevi, A. et al. Development of renewable energy fed three-level hybrid active filter for EV charging station load using Jaya grey wolf optimization. Sci Rep 14, 4429 (2024). https://doi.org/10.1038/s41598-024-54550-7

[24] Belqasem Aljafari, Yaswanth Kumar Alapati, Koganti Srilakshmi, Praveen Kumar Balachandran, Sudhakar Babu Thanikanti. "An optimized neural network-honey badger based control technique for a hybrid solar PV and battery energy storage fed unified power quality conditioner", Journal of Energy Storage, Volume 106, 2025, 114818, https://doi.org/10.1016/j.est.2024.114818.

[25] Srilakshmi K, Sundaragiri D, Gaddameedhi S, Vangalapudi R, Balachandran PK, Colak I and Selvarajan S (2024) Simulation of grid/standalone solar energy supplied reduced switch converter with optimal fuzzy logic controller using golden BallAlgorithm. Front. Energy Res. 12:1370412. doi: 10.3389/fenrg.2024.1370412

[26] Koganti S, Koganti KJ, Salkuti SR. Design of Multi-Objective-Based Artificial Intelligence Controller for Wind/Battery-Connected Shunt Active Power Filter. Algorithms. 2022; 15(8):256. https://doi.org/10.3390/a15080256

[27] Srilakshmi K, Rao GS, Balachandran PK and Senjyu T (2024) Green energy-sourced AI-controlled multilevel UPQC parameter selection using football game optimization. Front. Energy Res. 12:1325865. doi: 10.3389/fenrg.2024.1325865

[28] Srilakshmi K, Gummadi SR, Valluri N, Balachandran PK, Sangeetha K. Chimp algorithm based Solar-Hydrogen energy powered UPQC for distribution system. Energy Exploration & Exploitation. 2026;44(2):923-945. doi:10.1177/01445987251390554

[29] Subramaniyan, S., Vasantha Gowri, N., Srilakshmi, K., Balachandran, P. K., & Mohd Zainuri, M. A. (2025). Modified war strategy algorithm for optimal control and design of solar fed UPQC and power system state estimation problems. Journal of the Chinese Institute of Engineers, 1–17. https://doi.org/10.1080/02533839.2025.2574459

[30] Jyothi, K.K., Borra, S.R., Srilakshmi, K. et al. A novel optimized neural network model for cyber-attack detection using enhanced whale optimization algorithm. Sci Rep 14, 5590 (2024). https://doi.org/10.1038/s41598-024-55098-2.